Current Optics and Photonics
Vol. 1, No. 3, June 2017, pp. 239-246

ISSN: 2508-7266(Print) / ISSN: 2508-7274(Online)
DOI: https://doi.org/10.3807/COPP.2017.1.3.239

Design of a Plasmonic Switch Using Ultrathin Chalcogenide Phase-change Material

Seung-Yeol Lee*

Integrated plasmonics and optical device laboratory, Kyungpook National University, Buk-Gu Daehak-ro 80, Daegu 41566, Korea

(Received December 20, 2016 : revised February 4, 2017 : accepted February 6, 2017)

A compact plasmonic switching scheme, based on the phase change of a thin-film chalcogenide material ($Ge_2Sb_2Te_5$), is proposed and numerically investigated at optical-communication wavelengths. Surface plasmon polariton modal analysis is conducted for various thicknesses of dielectric and phase-change material layers, and the optimized condition is induced by finding the region of interest that shows a high extinction ratio of surface plasmon polariton modes before and after the phase transition. Full electromagnetic simulations show that multiple reflections inside the active region may conditionally increase the overall efficiency of the on/off ratio at a specific length of the active region. However, it is shown that the optimized geometrical condition, which shows generally large on/off ratio for any length of active region, can be distinguished by observing the multiple-reflection characteristic inside the active region. The proposed scheme shows an on/off switching ratio greater than 30 dB for a length of a few micrometers, which can be potentially applied to integrated active plasmonic systems.

Keywords : Surface plasmon polariton, Phase change material, Optical modulator, Fourier modal analysis
OCIS codes : (240.6680) Surface plasmon; (250.4110) Modulators; (310.2785) Guided wave applications; (230.7390) Waveguides, planar

I. INTRODUCTION

Over the few decades, surface plasmon polaritons (SPPs), which can be interpreted as a surface wave formed by the collective oscillation of photons and electrons at a metal-dielectric interface, are fascinated for realizing integrated optical systems, because of their unique optical properties such as strong light confinement and high sensitivity [1-3]. For example, it is known that the modal size of a propagating SPP is not restricted by the diffraction limit of light, because of its evanescently decaying modal shape in both metal and dielectric regions. Such highly confined modal characteristics of SPPs fascinate many researchers and inspire them to develop various kinds of integrated optical components, such as optical beam splitters [4], plasmonic-to-photonic interconnectors [5], ring-resonators [6], directional couplers [7], and even plasmonic switches [8-10] and ultra-compact lasers [11, 12].

Active plasmonic switching devices have been considered especially as one of the key technologies to realize an integrated plasmonic circuit system that can be controlled electro-optically or all-optically. Because of its significance in nanophotonics research, various approaches were demonstrated for active switching of SPP signals [13]. One of the earliest studies of an active plasmonic switch used the slow solid-liquid transition of gallium in Kretschmann's configuration [14], which observes the change of reflection power caused by SPP resonance shift [15]. After a few years, more compact and faster switching mechanisms appear for integrated plasmonic systems using absorption at activated quantum dots [16], photochromic transitions [8], nonlinear effect in metals subjected to femtosecond pulses [17], and the large refractive-index change of heavily doped transparent semiconductors driven by voltage [18, 19].

One of the promising techniques for achieving fast, repeatable optoelectronic switching characteristics is to use a phase-change material (PCM), such as vanadium dioxide (VO_2) or any of several chalcogenide compounds [20, 21].

*Corresponding author: seungyeol@knu.ac.kr

Color versions of one or more of the figures in this paper are available online.

In particular, it is known that some of the chalcogenide compounds composed of germanium (Ge), antimony (Sb), and tellurium (Te) provide a significant change in both electrical and optical characteristics during the phase transition [22]. Therefore, these compounds are not only used in conventional applications, such as optical data storage as in DVDs and phase-change memory (PRAM), but also for state-of-the-art nanotechnologies such as micro-imaging [23], tunable perfect absorbers [24], all-optically driven memory [25], photonic-crystal switch dividers [26], metasurfaces [27], and digital holography [28].

Although some of these previous works were assisted by SPP phenomena to achieve extraordinary optical characteristics, there has been almost no research for developing a compact switching device for the SPP signal itself, using a chalcogenide compound such as $Ge_2Sb_2Te_5$ (GST). Even though this phase-change material has so many benefits, such as rapid modulation [25], feasibility for highly integrated systems, possibility for both electrical and optical modulation [27, 29], and nonvolatile characteristics, there has not been much effort in using GST as a control material for SPP signals, because it is often considered to have very high losses.

In this manuscript, a mechanism for using GST as a compact plasmonic switch is proposed, applying an appropriately designed thin GST film capping on metal-dielectric SPP waveguide, instead of using GST directly as a lossy metal substrate. Using data for GST film permittivity from ellipsometry, the optimized GST film thicknesses for switching of a SPP signal within a compact modulation length are found. The significant change in the imaginary part of the permittivity during the GST phase transition can be proven to be a key mechanism for SPP on/off switching. Before and after the crystallization of capped GST, the modal power transmission of the proposed device is systematically analyzed by means of the Fourier modal analysis method (FMM).

II. DEVICE STRUCTURE AND MATERIAL PROPERTIES

The structure of the proposed device is shown in Fig. 1(a). On the surface of an Ag film, a thin dielectric layer is deposited for both inactive and active regions. In the active region, an additional thin film of phase-change material (GST) is capped on the dielectric film of length l_a. A dielectric layer may be needed for various reasons, such as thermal insulation of the upper GST layer from the metal heat sink, or optimization of the on/off switching ratio of the propagating SPP wave. For a given structure, an SPP mode launched from the inactive region may be transmitted, reflected, or scattered at the entrance to the active region, and the coupling coefficients of those light components can be altered through the phase change of GST. In Figs. 1(b) and (c), field distributions for the proposed scheme, optimized for an incident wavelength of 1550 nm are shown. It is clearly shown that the incident SPP wave can easily pass through the active region without significant scattering or attenuation, when the upper GST cap is in the amorphous state. On the other hand, when the GST changes to the crystalline phase, the attenuation of the SPP is significantly increased, so the SPP mode cannot be transmitted to the active region. This circumstance is not always realized for arbitrary geometrical conditions, though, and the latter part of this manuscript will discuss how the proposed structure can be optimized.

To use the proposed scheme as a plasmonic switch, the variation of GST permittivity caused by the phase transition should significantly affect the transmitted SPP. As reported for numerous other GST-based structures, the major phase transition of GST is caused by the crystallization and melting of molecular arrangements of GST [22-29]. For example, crystallization of GST often makes it much more reflective in the visible range, which has been a key mechanism in optical-memory applications [22]. In a recent

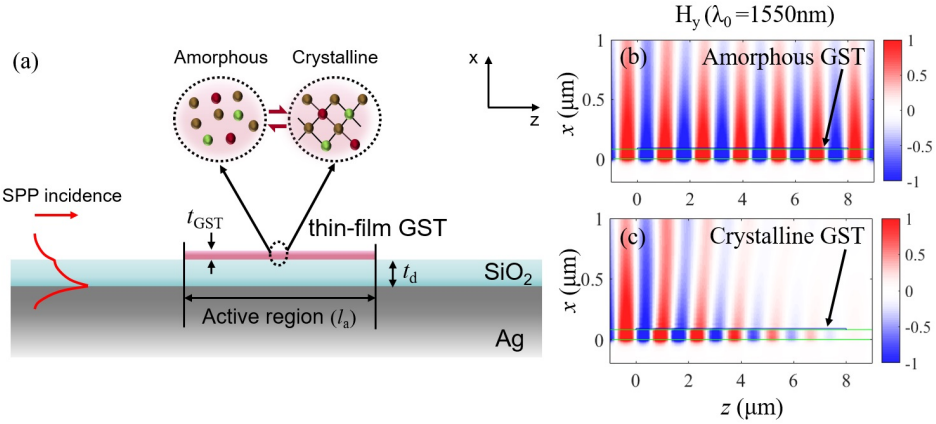

FIG. 1. (a) Schematic of the proposed plasmonic switch based on the phase change of thin-film GST. H_y field distribution of the proposed scheme at 1550 nm, when the GST capping is in (b) the amorphous state and (c) the crystalline state. t_d = 80 nm and t_{GST} = 10 nm are used in the simulations shown in (b) and (c).

TABLE 1. Refractive indices n and extinction coefficients k of GST and Ag at design wavelengths

Phase	1320 nm		1550 nm	
	n	k	n	k
Amorphous[a]	4.68	0.35	4.59	0.17
Crystalline[a]	7.04	2.72	6.88	2.11
Ag[b]	0.39	7.99	0.47	9.32

[a]Cited from [28], [b]Cited from [31].

demonstration, the permittivity of GST was measured with an ellipsometer, before and after the phase transition, from the visible to the near-infrared range [28]; these data are adapted to design the plasmonic switch proposed in this paper. According to the measurements, the extinction coefficient of GST can change significantly during the phase transition, especially in the infrared range, which is also verified by other studies [30]. Therefore, it seems quite reasonable to design the structure for the wavelengths frequently used in optical communication, 1320 nm and 1550 nm, which can also afford the propagating SPP wave a relatively long propagation length, compared to the visible region. The refractive indexes and extinction coefficients for silver, amorphous GST, and crystalline GST at the chosen wavelengths are summarized in Table 1.

III. SPP MODAL ANALYSIS OF THE PROPOSED STRUCTURE

Prior to investigating the full structure, SPP modal analyses of the inactive and active regions are performed. The inactive region can be interpreted as a trilayer Ag-dielectric-air waveguide, which has the analytic characteristic equation of [32]

$$(u_1+u_2)(u_3+u_2)-(u_1-u_2)(u_3-u_2)\exp(-2\kappa_2 d_2)=0 \quad (1)$$

where $u_i=\kappa_i/\varepsilon_i$ and t_d is the thickness of the dielectric layer. κ_i and ε_i indicate respectively the decay length of the SPP mode in the i^{th} layer and the relative permittivity of the i^{th} layer. In our case, $\varepsilon_1=\varepsilon_{Ag}=(n_{Ag}+j\mathrm{k}_{Ag})^2$, $\varepsilon_2=\varepsilon_{dielec}=2.25$, $\varepsilon_3=\varepsilon_{air}=1$ are used. The decay lengths can be expressed by

$$\kappa_i=\sqrt{\beta^2-\varepsilon_i k_0^2} \quad (i=1,2,3) \quad (2)$$

where k_0 is the free-space wave number of the incident light, and β is the complex wave number of the propagating SPP mode. By substituting Eq. (2) into (1), an equation with the single unknown value β is obtained, and the wave number of the SPP mode can be calculated by graphically finding the zero point of the substituted equation. The real and imaginary values of β contain information about the effective wavelength and the propagation length of the SPP mode respectively. For the case of the active region, a four-layered system should be considered (metal-dielectric-GST-air), which is more complicated than the inactive region. However, it is also possible to find the characteristic equations, and the solution can be found numerically.

If the incident free-space wavelength is fixed at 1320 nm or 1550 nm, the remaining sweep parameter for the inactive region is t_d, the thickness of the dielectric. In Figs 2(a) and (b), SPP modal characteristics such as effective refractive indices and propagation lengths for inactive region are shown for variable t_d. When t_d is increased to a certain value, it can be shown that the secondary SPP mode appears. For example, the secondary mode is observed when t_d is greater than 590 nm or 700 nm, for the cases of 1320-nm and 1550-nm incident light, respectively. If a given plasmonic waveguide becomes multimode, there may be unwanted mode transition at the abrupt interface of the inactive and active regions. Such a circumstance should be avoided, so the sweep range of the parameter t_d is restricted to 590 nm, and only the fundamental SPP mode will be

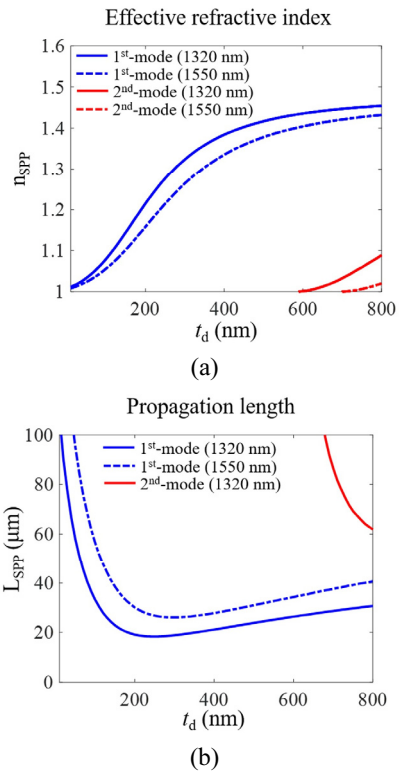

FIG. 2. (a) Effective refractive indices and (b) propagation lengths of SPP modes in the inactive region (silver-dielectric-air), at 1320 nm and 1550 nm. Blue lines indicate the values for the fundamental mode, whereas red lines indicate the values for the secondary mode. The propagation length of the secondary mode at 1550 nm is out of the viewing range, so it does not appear in (b).

analyzed from this point. It is also shown that the propagation length of the fundamental SPP mode rapidly increases for thinner values of t_d, when t_d is smaller than a certain value t_{min} that has a minimum propagation length. These t_{min} values are 230 nm and 290 nm, for 1320-nm and 1550-nm light respectively.

The modal characteristics of the active region at the design wavelength of 1320 nm, which are quite important to optimize the proposed plasmonic switch, are shown in Fig. 3. To analyze the modal characteristic of the active region, two optimization parameters t_d and t_{GST} should be simultaneously considered. It is shown that both the effective refractive indices and propagation lengths can be significantly changed by adding a thin capping layer of GST film, even just tens of nanometers thick. As shown in Figs. 3(a) and (b), the effective refractive indices gradually increase for thicker GST films, and the index change caused by varying GST film thickness is more dramatic when the dielectric film is sufficiently thin. This can be qualitatively explained by the energy portion of the SPP mode in the GST region, which gradually increases when thinner dielectric film is used. The refractive index of the SPP mode in the active region for the 1550-nm case is shown in Figs. 3(c) and (d), and shows a similar aspect for an incident wavelength of 1320 nm.

In Fig. 4(a), the ratio of propagation lengths before and after GST's phase transition ($L_{SPP,am}$ / $L_{SPP,cry}$) are shown for 1320 nm. A large difference in propagation length of the SPP mode before and after the phase transition of the GST film is apparent, especially in a specific region of t_d and t_{GST} conditions. It seems that t_d above 200 nm is not appropriate for a dramatic change in propagation length, because thick dielectric film reduces the effect of GST phase transition on SPP modal characteristics. Too thick t_{GST} is also inappropriate for a plasmonic switch, since the propagation lengths for both GST phase conditions are simultaneously reduced. Moreover, thicker GST film may significantly increase the difference in n_{SPP} between the inactive and active regions; therefore the coupling efficiency from inactive to active regions can also decrease, which must be avoided to optimize the plasmonic switch. Similar propagation-length aspects are also observed at the other design wavelength of 1550 nm, which can be seen in Fig. 4(b). In this case, the optimum thicknesses are slightly shifted to larger values, and the maximum value of the propagation-length ratio becomes larger than in the 1320-nm case.

From modal analysis of the active region, it is possible to roughly determine the region of thickness conditions exhibiting a large difference in SPP propagation lengths. However, the value of $L_{SPP,am}$ / $L_{SPP,cry}$ does not give an exact condition for an optimized device, because other factors, such as coupling efficiency of the SPP mode from the inactive to the active region, multiple reflections inside

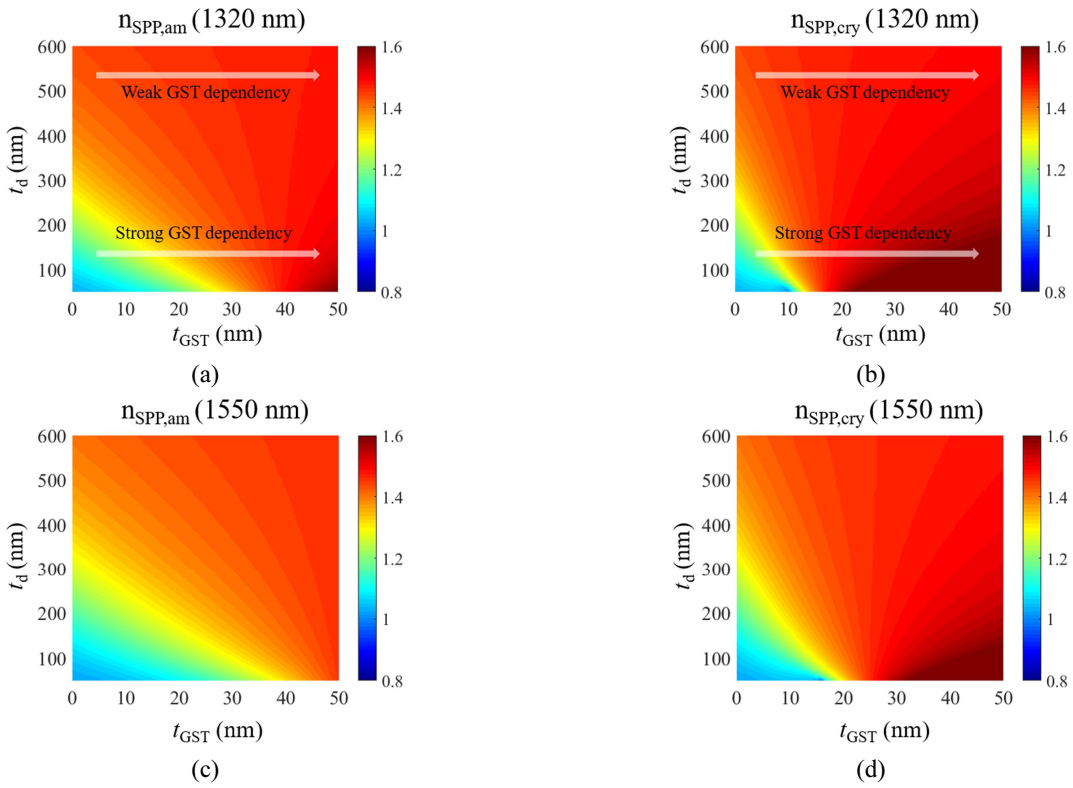

FIG. 3. n_{SPP} of the active region (silver-dielectric-GST-air) at 1320 nm, for (a) amorphous and (b) crystalline GST capping. n_{SPP} of the active region at 1550 nm, for (c) amorphous and (d) crystalline GST capping.

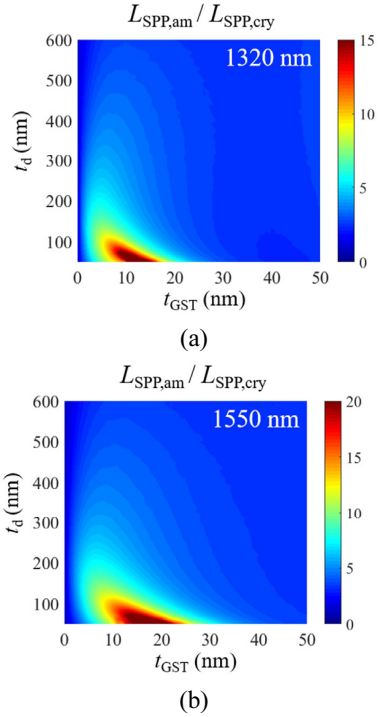

FIG. 4. The ratio of L_{SPP} for the active region (silver-dielectric-GST-air) at incident wavelengths of (a) 1320 nm and (b) 1550 nm.

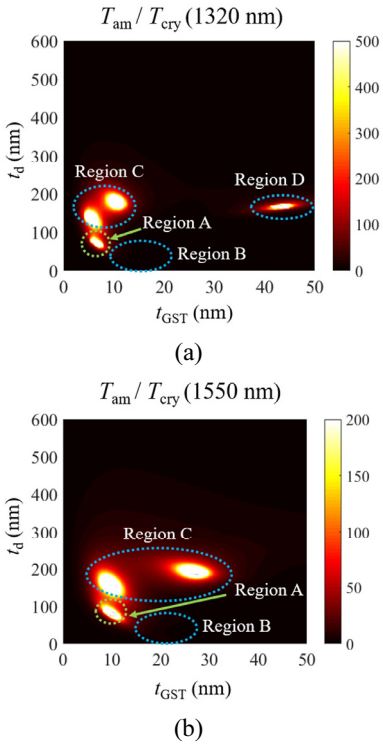

FIG. 5. The ratio of modal transmittance at (a) 1320 nm and (b) 1550 nm for the full structure shown in FIG. 1. The length l_a of the active region is fixed to 8 μm in this simulation.

the active region, and scattering at the junction of inactive and active regions, can affect the overall transmittance. Therefore, in the next section full numerical simulations of the structure shown in Fig. 1 are conducted, using the Fourier modal method (FMM).

IV. ANALYSIS OF POWER COUPLING EFFICIENCY

The FMM is a powerful analysis method, especially for calculating the power coupling ratio for a specific mode. This method analyzes the geometric shape of a layer with finite numbers of Fourier coefficients, then find the eigenmodes, eigenvalues, and coupling coefficients for the electromagnetic vectors. The detailed method and MATLAB code for FMM simulation can be found in [33, 34]. The input signal is given as an SPP mode incident from the left side of the inactive region, which can be launched using the slit-coupling method [35] or Kretschmann's configuration [36]. The modal reflectance R and transmittance T are defined by the reflected power coupled to the same mode as the input SPP at the left side of the junction, and the transmitted power coupled to the same mode at the right side of the junction, respectively, which are normalized by the input power at the left side of the junction.

Figure 5(a) shows the ratio of modal transmittance before and after the GST phase transition (T_{am} / T_{cry}) varying with two thicknesses (t_d and t_{GST}) at 1320 nm. The length l_a of the active region is fixed at 8 μm in this simulation, and will be tuned for specific cases later. As shown in Fig. 5(a), there are several optimized rconditions for a high modal transmittance ratio, which are mainly observed in Regions A, C, and D. Region A shows both high performance in the modal analysis and the full numerical simulation, whereas Regions C and D show high performance only in the full numerical simulation, with relatively low performance in the modal analysis. Region B shows the best performance in the modal analysis, as shown in Fig. 4(a), but it does not provide high performance in the full numerical simulation. Similar aspects can be observed for an incident wavelength of 1550 nm, as depicted in Fig. 5(b), except for the shift of optimized conditions to larger geometry. Therefore, Region D disappears from the scope of the parametric sweep at 1550 nm. The field distributions in these parametric regions will be investigated in the next paragraph.

In Figs. 6(a)-(h), the H_y field distributions for the proposed scheme (at 1320 nm), before and after the GST phase transition, are shown for representative conditions selected from Regions A, B, C, and D respectively. The representative conditions of Regions A, C, and D are chosen according to the local maximum of the bright spot shown in Fig. 5(a), whereas that of Region B is appropriately chosen from Fig. 4(a). As depicted in Figs. 6(a)

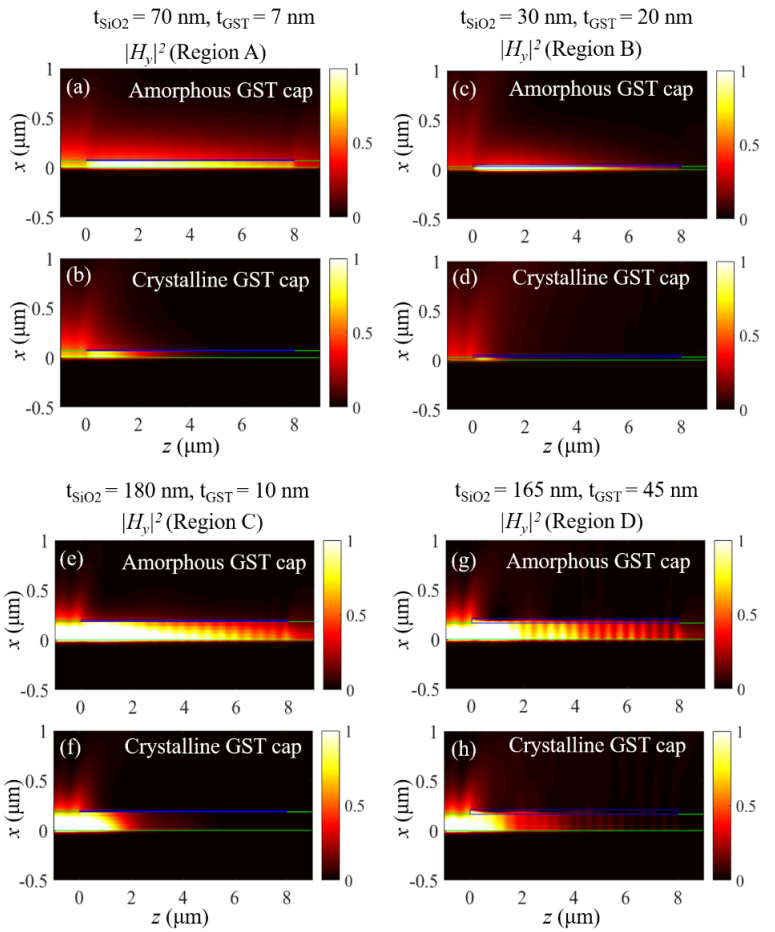

FIG. 6. H_y field distribution for the proposed plasmonic switching scheme, for different geometric conditions selected from Regions A((a) and (b)), B((c) and (d)), C((e) and (f)), and D((g) and (h)). Figures (a), (c), (e), and (g) show the field distributions when the GST layer is in the amorphous state, whereas (b), (d), (f), and (h) show the cases when the GST film is crystalline.

and 6(b), the GST phase transition under the parametric conditions of Region A (t_{SiO2} = 70 nm, t_{GST} = 7 nm) can dramatically change the propagation characteristics of the SPP mode. Moreover, it seems that the modal reflection and multiple reflections of the SPP mode within the active region is quite small, compared to the cases of Region C (t_{SiO2} = 180 nm, t_{GST} = 10 nm) and Region D (t_{SiO2} = 165 nm, t_{GST} = 45 nm).

On the other hand, the field distributions for Region B (t_{SiO2} = 30 nm, t_{GST} = 20 nm), which shows the best performance in the modal analysis but relatively poor performance in the full simulation, are shown in Figs. 6(c) and (d). Although the attenuation of the SPP mode for crystalline GST capping (Fig. 6(d)) is much stronger than the case shown in Fig. 6(b), the coupling of the SPP mode at the end of the active region is quite small for amorphous GST capping (Fig. 6(c)), compared to the case shown in Fig. 6(a). Such degradation may be caused by too great a difference in SPP modal shape between the inactive and active regions. Therefore, the ratio of overall modal transmittance becomes worse, compared to the case for Region A.

In Figs. 6(e)-(h), the field distributions for other high-performance conditions shown in Regions C and D are shown. Although Region C has two local maxima, only one of those conditions is shown, as they show similar field distributions. The standing-wave patterns shown in these figures indicate that there are strong multiple reflections inside the active region when t_{SiO2} is too thick. Under these conditions, the high ratio of modal transmittance mainly originates from cavity resonance of the active region, rather than the difference in extinction coefficients between amorphous and crystalline GST. Since the cavity-resonance condition strongly depends on the length of cavity, these kinds of conditions may apply for the specific length of l_a = 8 μm, but cannot be generally used for an arbitrary value of l_a. Therefore, it can be expected that the conditions of Region A may be the best candidate for the proposed plasmonic switching device controlled by GST phase transition.

To verify the assumption that the optimized condition of Region A shows less sensitivity for a change in l_a, Fig. 7 plots the variation of modal transmission ratio with length of the active region, for representative conditions of Regions A, B, C, and D. As already checked in Fig. 5,

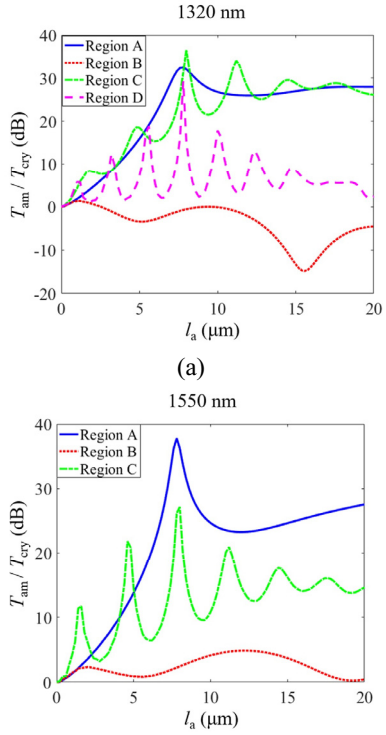

FIG. 7. The ratio of modal transmittance (in dB) is plotted for varying length of active region, at (a)1320 nm and (b)1550 nm.

the representative conditions of Regions A, C, and D show a very high modal transmission ratio of ~30 dB (~1000) at the specific length of $l_a = 8$ μm. However, significant fluctuation in performance is observed for the conditions of C and D, which is clear evidence of multiple reflections inside the active region. It is quite important to reduce multiple reflections in using the proposed scheme as a compact optical modulator, because multiple reflections can distort the output signal when a pulsed input signal is used.

The best performance of the proposed device is observed near $l_a = 8$ μm, but the device still has a reasonably high on/off ratio greater than 10 dB at $l_a = 3$ μm; this optical modulation length is quite short (about twice the SPP wavelength), so the proposed device can be termed a 'compact' plasmonic modulator driven by a phase-change material. The proposed scheme has quite a simple configuration and can be fabricated by conventional photolithography, and very thin (~7 nm) GST film can be deposited by sputtering [28]. The phase change of the GST film may be induced by flowing electrical current through metal electrodes connected to the thin GST film, as demonstrated recently [28]. Similar processes can also be carried out for a different design wavelength of 1550 nm, shown in Fig. 7(b). The field distributions of the optimized device at 1550 nm ($t_{SiO2} = 80$ nm, $t_{GST} = 10$ nm, $l_a = 8$ μm) show better performance then in the case of 1320 nm, and were depicted in Figs. 1(b) and (c) as a representative figure.

Finally, the stability of the optimized conditions with respect to a small change in extinction coefficient is briefly analyzed. For example, Region A, which has the best performance at 1320 nm, has a modal transmission ratio of 32.08 dB for the simulated conditions. A 10% reduction in the extinction coefficient of crystalline GST gives a 30.4 dB modal transmission ratio. The degradation of optimized performance due to instability of the permittivity is not so significant. Other perturbations, such as a 10% change in the extinction coefficient of amorphous GST, show less variation (a result of 31.9 dB) than does a change in the crystalline GST's extinction coefficient.

V. CONCLUSION

In conclusion, a compact plasmonic switching scheme based on GST phase transition is proposed and optimized at optical communication frequencies. It is shown that the difference in SPP mode extinction before and after the phase change of a thin GST film deposited on a metal-dielectric substrate is a primary factor for the high on/off ratio of the proposed scheme. Full electromagnetic simulations based on FMM show that multiple reflections inside the cavity formed by the active region can affect the on/off ratio. However, only the geometric conditions that simultaneously satisfy low multiple reflections and high ratio of SPP modal extinction show generally large on/off ratio, for any length of active region. The optimized conditions for the proposed device may have a very high on/off ratio of ~30 dB with a modulation length of a few micrometers, at two chosen wavelengths for optical communication. Since the phase transition of GST can be induced either optically or electrically, the proposed scheme is expected to be a simple but promising technique for developing integrated optical systems.

ACKNOWLEDGMENT

This research was supported by the Kyungpook National University Research Fund, 2016.

REFERENCES

1. W. L. Barnes, A. Dereux, and T. W. Ebbesen, "Surface plasmon subwavelength optics," Nature **424**, 824-830 (2003).
2. T. W. Ebbesen, H. J. Lezec, H. F. Ghaemi, T. Thio, and P. A. Wolff, "Extraordinary optical transmission through sub-wavelength hole arrays," Nature **391**, 667-669 (1998).
3. B. Lee, S. Kim, H. Kim, and Y. Lim, "The use of plasmonics in light beaming and focusing," Prog. Quant. Electron. **34**, 47-87 (2010).
4. S.-Y. Lee, J. Park, I. Woo, N. Park, and B. Lee, "Surface plasmon beam splitting by the photon tunneling through the

plasmonic nanogap," Appl. Phys. Lett. **97**, 133113 (2010).
5. S.-Y. Lee, J. Park, M. Kang, and B. Lee, "Highly efficient plasmonic interconnector based on the asymmetric junction between metal-dielectric-metal and dielectric slab waveguides," Opt. Express **19**, 9562-9574 (2011).
6. S. I. Bozhevolnyi, V. S. Volkov, E. Devaux, J.-Y. Laluet, and T. W. Ebbesen, "Channel plasmon subwavelength waveguide components including interferometers and ring resonators," Nature **440**, 508-511 (2006).
7. M. Z. Alam, J. Niklas Caspers, J. S. Aitchison, and M. Mojahedi, "Compact low loss and broadband hybrid plasmonic directional coupler," Opt. Express **21**, 16029-16034 (2013).
8. R. A. Pala, K. T. Shimizu, N. A. Melosh, and M. L. Brongersma, "A nonvolatile plasmonic switch employing photochromic molecules," Nano Lett. **8**, 1506-1510 (2008).
9. J. Lin, J. P. B. Mueller, Q. Wang, G. Yuan, N. Antoniou, X.-C. Yuan, and F. Capasso, "Polarization-controlled tunable directional coupling of surface plasmon polaritons," Science **340**, 331-334 (2013).
10. S.-Y. Lee, K. Kim, S.-J. Kim, H. Park, K.-Y. Kim, and B. Lee, "Plasmonic meta-slit: shaping and controlling near-field focus," Optica **2**, 6-13 (2015).
11. R. F. Oulton, V. J. Sorger, T. Zentgraf, R.-M. Ma, C. Gladden, L. Dai, G. Bartal1, and X. Zhang, "Plasmon lasers at deep subwavelength scale," Nature **461**, 629-632 (2009).
12. T. P. H. Sidiropoulos, R. Röder, S. Geburt, O. Hess, S. A. Maier, C. Ronning, and R. F. Oulton, "Ultrafast plasmonic nanowire lasers near the surface plasmon frequency," Nature Physics **10**, 870-876 (2014).
13. K.F. MacDonald and N.I. Zheludev, "Active plasmonics: current status," Laser Photon. Rev. **4**, 562-567 (2010).
14. A. V. Krasavin, A. V. Zayats, and N. I. Zheludev, "Active control of surface plasmon-polariton waves," J. Opt. A: Pure Appl. Opt. **7**, S85-S89 (2005).
15. S. Roh, T. Chung, and B. Lee, "Overview of the characteristics of micro- and nano-structured surface plasmon resonance sensors," Sensors **11**, 1565-1588 (2011).
16. D. Pacifici, H. J. Lezec, and H. A. Atwater, "All-optical modulation by plasmonic excitation of CdSe quantum dots," Nat. Photon. **1**, 402-406 (2007).
17. K. F. MacDonald, Z. L. Sámson, M. I. Stockman, and N. I. Zheludev, "Ultrafast active plasmonics," Nat. Photon. **3**, 55-58 (2009).
18. Y. W. Huang, H. W. Lee, R. Sokhoyan, K. Thyagarajan, R. Pala, S. Han, D. P. Tsai, and H. A. Atwater, "Gate-tunable conducting oxide metasurfaces," Nano Lett. **16**, 5319-5325 (2016).
19. H. W. Lee, G. Papadakis, S. P. Burgos, K. Chander, A. Kriesch, R. Pala, U. Peschel, and H. A. Atwater, "Nanoscale conducting oxide plasMOStor," Nano Lett. **14**, 6463-6468 (2014).
20. M. Seo, J. Kyoung, H. Park, S. Koo, H.-S. Kim, H. Bernien, B. J. Kim, J. H. Choe, Y. H. Ahn, H.-T. Kim, N. Park, Q-H. Park, K. Ahn, and D.-S. Kim, "Active terahertz nano-antennas based on VO2 phase transition," Nano Lett. **10**, 2064-2068 (2010).
21. K. Appavoo and R. F. Haglund, "Detecting nanoscale size dependence in VO2 phase transition using a split-ring resonator metamaterial," Nano Lett. **11**, 1025-1031 (2011).
22. A. V. Kolobov, P. Fons, A. I. Frenkel, A. L. Ankudinov, J. Tominaga, and T. Uruga, "Understanding the phase-change mechanism of rewritable optical media," Nat. Material **3**, 703-708 (2004).
23. P. Hosseini, C. D. Wright, and H. Bhaskaran, "An opto-electronic framework enabled by low-dimensional phase-change film," Nature **511**, 206-211 (2014).
24. A. Tittl, A. U. Michel, M. Schäferling, X. Yin, B. Gholipour, L. Cui, M. Wuttig, T. Taubner, F. Neubrech, and H. Giessen, "A switchable mid-infrared plasmonic perfect absorber with multispectral thermal imaging capability," Advanced Material **27**, 4597-4603 (2015).
25. C. Ríos, M. Stegmaier, P. Hosseini, D. Wang, T. Scherer, C. D. Wright, H. Bhaskaran, and W. HP. Pernice, "Integrated all-photonic non-volatile multi-level memory," Nature Photon. **9**, 725-733 (2015).
26. B. Ma, P. Zhang, H. Wang, T. Zhang, J. Zeng, Q. Zhang, G. Wang, P. Xu, W. Zhang, and S. Dai, "Photonic-crystal switch divider based on $Ge_2Sb_2Te_5$ thin films," Appl. Opt. **55**, 9205-9210 (2016).
27. Q. Wang, E. T. F. Rogers, B. Gholipour, C.-M. Wang, G. Yuan, J. Teng, and N. I. Zheludev, "Optically reconfigurable metasurfaces and photonic devices based on phase change materials," Nat. Photon. **10**, 60-65 (2016).
28. S.-Y. Lee, Y.-H. Kim, S.-M Cho, G. H. Kim, T.-Y. Kim, H. Ryu, H. N. Kim, H. B. Kang, C.-Y. Hwang, and C.-S. Hwang, "Holographic image generation with a thin-film resonance caused by chalcogenide phase-change material," Sci. Rep. doi: 10.1038/srep41152 (2017).
29. C. H. Chu, M. L. Tseng, J. Chen, P. C. Wu, Y.-H. Chen, H.-C. Wang, T.-Y. Chen, W. T. Hsieh, H. J. Wu, G. Sun, and D. P. Tsai, "Active dielectric metasurface based on phase-change medium," Laser Photon. Rev. doi: 10.1002/lpor.201600106 (2016).
30. J.-W. Park, S. H. Eom, H. Lee, J. L. F. Da Silva, Y.-S. Kang, T.-Y. Lee, and Y. H. Khan, "Optical properties of pseudo binary GeTe, $Ge_2Sb_2Te_5$, $GeSb_2Te_4$, $GeSb_4Te_7$, and Sb_2Te_3 from ellipsometry and density functional theory," Phys. Rev. B **80**, 115209 (2009).
31. E. D. Palik, *Handbook of Optical Constants of Solids* (Academic Press, New York, 1991).
32. J. Park, K.-Y. Kim, I.-M. Lee, and B. Lee, "Complete tunneling through the surface mode in a metal-insulator-metal waveguide," J. Korean Phys. Soc. **66**, 929-934 (2015).
33. H. Kim, I.-M. Lee, and B. Lee, "Extended scattering-matrix method for efficient full parallel implementation of rigorous coupled-wave analysis," J. Opt. Soc. Am. A **24**, 2313-2327 (2007).
34. H. Kim, J. Park, and B. Lee, *Fourier modal method and its application in computational nanophotonics*, (CRC Press, New York, 2012).
35. S.-Y. Lee, I.-M. Lee, J. Park, S. Oh, W. Lee, K.-Y. Kim, and B. Lee, "Role of magnetic induction currents in nanoslit excitation of surface plasmon polaritons," Phys. Rev. Lett. **108**, article 213907 (2012).
36. S. Roh, T. Chung, and B. Lee, "Overview of the characteristics of micro- and nano-structured surface plasmon resonance sensors," Sensors **11**, 1565-1588 (2011).